ELSEVIER

Journal of Nuclear Materials 295 (2001) 1–15

journal of nuclear materials

www.elsevier.nl/locate/jnucmat

Effect of bonding and bakeout thermal cycles on the properties of copper alloys irradiated at 350°C

B.N. Singh [a,*], D.J. Edwards [b], M. Eldrup [a], P. Toft [a]

[a] *Materials Research Department, Risø National Laboratory, Roskilde DK-4000, Denmark*

[b] *Materials Development Group, MSIN P8-15, Pacific Northwest National Laboratory, Richland WA 99352, USA*

Received 14 November 2000; accepted 17 February 2001

Abstract

Screening experiments were carried out to determine the effect of bonding and bakeout thermal cycles on microstructure, mechanical properties and electrical resistivity of the oxide dispersion strengthened (GlidCop, CuAl-25) and the precipitation hardened (CuCrZr, CuNiBe) copper alloys. Tensile specimens were given heat treatments corresponding to solution anneal, prime-aging, bonding thermal treatment followed by re-aging and the reactor bakeout treatment. A number of specimens were irradiated at 350°C to a dose level of ≃0.3 dpa in the DR-3 reactor at Risø. Both unirradiated and irradiated specimens were tensile tested at 350°C. The microstructure and electrical resistivity were determined in the unirradiated and irradiated conditions. The post-deformation microstructure and fracture surfaces of unirradiated and irradiated specimens were examined. The main results are described and their salient features discussed. The most significant effect of neutron irradiation is a severe loss of ductility in the case of CuNiBe alloys.

1. Introduction

Copper alloys are being considered as heat sink materials in the first wall and divertor assemblies of International thermonuclear experimental reactor (ITER) because of their good thermal conductivity [1,2]. The oxide dispersion strengthened (ODS) copper alloys (e.g., GlidCop® CuAl-25) have long been considered the primary candidate class of alloys due to their superior microstructural stability and swelling resistance during irradiation when compared to precipitation strengthened alloys such as CuCrZr and CuNiBe. Recently, however, it has become increasingly clear that each of the alloys has advantages over the other alloys depending on the operating parameters/requirements, irradiation dose levels and the initial state of the alloy. Implicit in this statement is the effect of the bonding treatment used to join the copper alloy to both the armour (Be, W, or C) and the stainless steel structure that will handle the structural loading.

Low dose screening experiments were initiated on all three candidate alloys. The goal of the experiments was twofold: first, to help understand what effect the joining treatment might have on the performance of these alloys after irradiation at various temperatures, and secondly, to narrow the number of alloys to two alloys, one main alloy and its backup. A series of heat treatments were given to CuCrZr, CuNiBe, and CuAl-25 to simulate the effect of possible joining treatments such as hot isostatic pressing. The first set of irradiation experiments on these specimens was recently completed and the results were reported on the effect of various heat treatments on the mechanical properties, electrical resistivity and microstructure of CuCrZr, CuNiBe and CuAl-25 both before and after irradiation at 100°C and 250°C to 0.3 dpa [3,4].

The present report summarises the results of a second set of experiments on the same materials irradiated to the same dose of 0.3 dpa, but at 350°C instead. The effect of the various heat treatments described herein on the unirradiated microstructure has been reported pre-

* Corresponding author. Tel.: +45-46 775 709; fax: +45-46 775 758.

E-mail address: bachu.singh@risoe.dk (B.N. Singh).

0022-3115/01/$ - see front matter
PII: S0022-3115(01)00507-4

viously [4], and will not be presented in this report in detail. Tensile properties of unirradiated and irradiated specimens with various heat treatments tested at 350°C are described. The results of electrical resistivity measurements at 23°C are also presented. The effect of irradiation on the microstructure of the various alloys is illustrated with representative micrographs. The implications of these results are briefly discussed.

2. Materials and experimental procedure

The materials used in the present investigations were CuCrZr, CuNiBe and Cu–Al_2O_3 alloys. The CuCrZr and CuNiBe alloys were supplied by Tréfimétaux (France) in the form of 20 mm thick plates. In addition, Hycon 3HP™ (heat number 33667), a CuNiBe alloy produced by Brush Wellman (USA), was also included in the present study. The ODS copper alloy (i.e., Cu–Al_2O_3) GlidCop™ CuAl-25 was supplied by OGM Americas (formerly SCM Metals) in the form of rods in the as-extruded (i.e., wrought) condition. Henceforth, the ODS copper (Cu–Al_2O_3) will be referred to as CuAl-25. The chemical composition of these alloys is listed in Table 1. The exact composition of the Hycon alloy is held as proprietary information by Brush Wellman, but the alloy is similar in overall composition to the Tréfimétaux CuNiBe.

Flat tensile specimens (gauge length = 7.0 mm) were cut from cold-rolled (≈80%) sheets (≈0.3 mm thick) of the Tréfimétaux CuCrZr and CuNiBe alloys, and from the as-received block of Hycon 3HPTM. Round tensile specimens of CuAl-25 (of gauge diameter 3 mm) were machined from the as-supplied rod, which was in the as-wrought condition (i.e., no additional cold-work after extrusion).

Table 1
Chemical composition of copper alloys

OFHC–Cu	Cu – 10, 3, 1 and <1 ppm of Ag, Si, Fe and Mg, respectively
CuCrZr	Cu – 0.8% Cr, 0.07% Zr, 0.01% Si
CuNiBe	Cu – 1.75% Ni, 0.45% Be
CuAl25	Cu – 0.25% Al as oxide particles (0.46% Al_2O_3)

For the screening experiments, the tensile specimens of Tréfimétaux CuCrZr and CuNiBe were given the five different heat treatments (A, B, E, C and C′) listed in Table 2. The bonding thermal heat treatment for CuAl-25 specimens consisted of annealing at 950°C for 30 min (referred to as heat treatment D). The bakeout treatment was not given to the CuAl-25 since it is well known that this temperature has little effect on microstructure and properties of the alloy. All heat treatments were carried out in vacuum ($<10^{-8}$ bar). The details of the proprietary heat treatment of the Hycon alloy are not known, but the alloy is essentially in a fully hardened condition (HT temper designation). It was irradiated in the as-received condition. The effect of the various heat treatments on the overall grain structure and grain size for both the Tréfimétaux CuNiBe and CuCrZr is described in [4].

Tensile specimens of CuCrZr, CuNiBe, Hycon, and CuAl-25 alloys with the different heat treatments were irradiated at 350°C in the DR-3 reactor at Risø in the high-temperature rig. During irradiation, temperature was measured, controlled (within ±2°C) and recorded continuously. All specimens were irradiated at the same time to a fluence level of 1.5×10^{24} n/m^2 ($E > 1$ MeV), which corresponds to a displacement dose level of ≃0.3 dpa (NRT). The neutron flux during irradiation was approximately 2.5×10^{17} n/m^2 ($E > 1$ MeV) which corresponds to a displacement damage rate of $\simeq 5 \times 10^{-8}$ dpa (NRT)/s.

Both unirradiated and irradiated tensile specimens (at least two specimens from each condition) were tested in an Instron machine at a strain rate of 1.2×10^{-3} s^{-1}. Tensile tests were carried out at 350°C in vacuum ($<10^{-7}$ bar). The test temperature of 350°C was reached within 30 min. The cross-head displacement was measured and

Table 2
Summary of bonding and bakeout heat treatments for CuCrZr, CuNiBe and CuAl-25 alloys

Type	Heat treatment
Hycon	Proprietary, but essentially solution annealed, quenched, cold-worked, and aged to produce an HT temper condition
A	Solution annealing at 950°C for 1 h followed by water quench
E	Prime-aging: heat treatment A + aging at 475°C for 30 min followed by water quench
B	Bonding thermal cycle: heat treatments A + E + annealing at 950°C for 30 min followed by furnace cooling + re-aging at 475°C for 30 min followed by furnace cooling
C	Bakeout thermal cycle: heat treatment B + annealing at 350°C for 100 h followed by furnace cooling
C′	Bakeout thermal cycle: heat treatment E + annealing at 350°C for 100 h followed by furnace cooling
D	Annealing at 950°C for 30 min (only for CuAl-25)
D′	CuAl-25 in the as-wrought condition, i.e., without any heat treatment

used to determine the stress–strain behaviour of the specimens.

For transmission electron microscopy (TEM) investigations, 3 mm discs were punched from the unirradiated and irradiated sheet tensile specimens and thinned mechanically to ≃0.1 mm thickness. The TEM specimens from the as-wrought CuAl-25 tensile specimens were cut from the gauge sections perpendicular to the tensile axis, and thinned mechanically to ≃0.1 mm. These discs were then twin-jet electropolished in a solution of 25% perchloric acid, 25% ethanol and 50% water at 11 V for about 15 s at ≃20°C. Specimens were examined in a JEOL 2000 FX transmission electron microscope. The fracture surfaces of the irradiated as well as unirradiated specimens were examined in JEOL 840 scanning electron microscope.

All analyses of stacking fault tetrahedra (SFT's) density and size distribution were performed on micrographs taken in a (g, +4g) or (g, +5g) weak beam dark field (WBDF) condition approximately 8° off the $\langle 0\,1\,1\rangle$ zone axis, with $g = [2\,0\,0]_{Cu}$ being the operating diffraction condition. The micrographs were taken in regions near the edge of the foil 15–25 nm in thickness. Thickness was determined by counting WBDF fringes. All measurements were taken from micrographs with a total magnification of at least 600 000. Details of the analysis of the oxide particles in CuAl-25 and of the precipitates in CuCrZr and CuNiBe alloys are described in [4] and will not be repeated here. The density and size of SFT's could not be determined in any of the CuNiBe alloys due to the high density of precipitates.

All resistivity measurements were made at room temperature (23°C) (see [4] for details). The total uncertainty on each measurement was estimated to be less than 3%. The average resistivity of OFHC-copper (annealed at 550°C for 2 h) was found to be 1.682 μΩ cm, which is in good agreement with the nominal resistivity of copper at room temperature of 1.698 μΩ cm. The relative resistivity (RR) of the alloys was calculated from the following relationship: $RR = R \times t \times w/(R_{Cu} \times t_{Cu} \times w_{Cu})$, where R is the electrical resistance measured for the specimen of thickness t and width w. The index Cu refers to the values for the reference OFHC–Cu sample.

3. Experimental results

3.1. Microstructure of unirradiated Hycon 3HP™

The unirradiated Hycon alloy appears to possess a microstructure similar to that of the Tréfimétaux CuNiBe in the HTE condition. Both alloys contain a number of large Ni-rich beryllide particles [5–7], and there are a few unidentified smaller particles located at the grain boundaries. However, the Hycon alloy does not show any evidence of the precipitate denuded zones along the grain boundaries observed in the Tréfimétaux CuNiBe (HTE) [4]. In addition, the large primary Ni-rich beryllide particles shown in Figs. 1(a) and (b) have recrystallised regions around the primary particles. This is thought to be the result of a high dislocation density around the particles as a result of the cold-working, leading to recrystallisation during the aging treatment. Fig. 1(b) shows that the recrystallised region contains a low density of round or oblong precipitates much different from the γ'' precipitates present in the interiors of the grains. These precipitates have not been identified.

The interiors of the grains contain a high density of γ'' precipitates, examples of which are shown in Fig. 1(c).

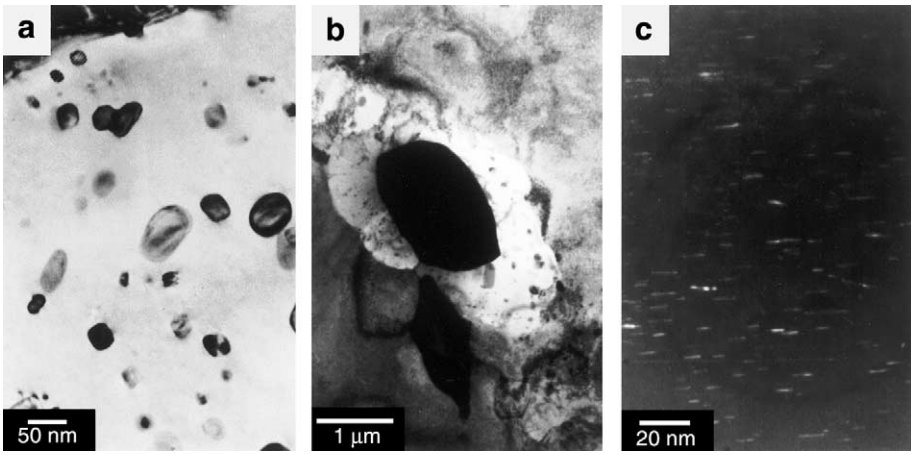

Fig. 1. Microstructure of the unirradiated Hycon 3HP (heat number 33667) showing (a) a close-up of the recrystallised region and the smaller particles, (b) an example of a recrystallised region around a large beryllide. The γ'' precipitates shown in (c) were imaged in the precipitate dark field contrast.

Table 3
Precipitate and particle densities in copper alloys with pre-irradiation heat treatments A, E, B, C, C′ and D[a]

Heat treatments	Tréfimétaux CuCrZr	Tréfimétaux CuNiBe	Hycon 3HP	CuAl-25
Pre-irradiation precipitate microstructure (10^{23} m^{-3})[b]				
A	–	–	–	–
E	0.59 (2.9 nm)[c]	18 (3.8 nm)[d]	2.4 (10 nm)	–
B	0.36 (2.3 nm)[c]	14 (6.6 nm)[d]	–	–
C	–	13	–	–
C′	0.51	13	–	–
D	–	–	–	0.19 (6.4 nm)
Post-irradiation microstructure – 350°C, 0.3 dpa (10^{23} m^{-3})				
A	1.3 (2.3 nm)[e]	6.9 (3.9 nm)[d]	–	–
E	1.8 (4.3 nm)[f]	6.3 (4.9 nm)[d]	1.8 (10.8 nm)	–
B	0.29 (5.4 nm)[f]	4.2 (7.4 nm)[d]	–	–
D	–	–	–	0.18 (9.4 nm)

[a] Alloys were irradiated at 350°C to a dose level of ≈0.3 dpa.
[b] All results for the unirradiated microstructure except for the unirradiated Hycon were reported in [4].
[c] Average size as given is from the measurement of the line of no contrast present for the small spherical precipitates possessing the lobe–lobe contrast.
[d] Average precipitate diameter assuming round platelets.
[e] Average size for the largest fringe on unidentified precipitates.
[f] Average size is measured from incoherent fringed precipitates.

These precipitates have also been observed in Tréfimétaux CuNiBe alloys, along with GP zones. GP zones do not appear to be present in the Hycon alloy, since the diffraction patterns do not show evidence of the streaking commonly visible along the $[200]_{Cu}$ directions in the diffraction patterns when a high density of GP zones is present. Instead, discrete reflections at 1/3 and 2/3$[200]_{Cu}$ are present, which are attributed to the γ'' phase according to the work of Guha [5]. The average precipitate size is given in Table 3 as $\simeq$10 nm with a density of 2.4×10^{23} m^{-3}. The size distributions for the γ'' precipitates in the unirradiated Hycon are provided in Fig. 2(a), showing that the precipitate size ranges from less than 3 nm to larger than 20 nm. The average size in the Hycon alloy is therefore much larger than that reported in the unirradiated Tréfimétaux CuNiBe in either the HTE or the HTB condition, and the density is less by a factor of 7 or more. Note that even in Hycon with its coarser microstructure the precipitate density is much higher than that measured for the unirradiated CuCrZr and CuAl-25 (Table 3).

3.2. Post-irradiation microstructure

None of the copper alloys examined show any evidence of void swelling. However, each alloy responds differently to the effects of neutron irradiation at 350°C. The details of the microstructural analysis are presented in the following sections, and where appropriate, comparisons are made with the microstructures of the unirradiated and 100°C and 250°C irradiated materials reported in [3] and [4]. The cluster density was found to be $\simeq 1 \times 10^{22}$ m^{-3} for the CuCrZr alloys, and $\simeq 8 \times 10^{20}$ m^{-3} for the CuAl-25. The cluster density could not be measured for the CuNiBe alloys due to the high precipitate density.

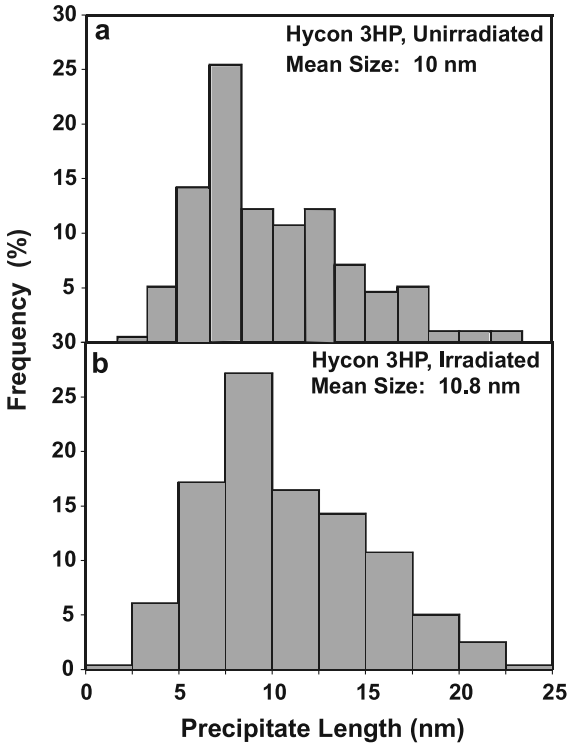

Fig. 2. Measured precipitate size distributions of Hycon 3HP in the unirradiated and irradiated conditions. Note that irradiation causes little changes in the size distribution.

3.2.1. Hycon 3HP™

An example of the post-irradiation microstructure is shown in Fig. 3. No precipitate denuded zones along the grain boundaries or in the vicinity of the primary beryllides were observed. More of the small precipitates were observed at the boundaries as shown in Fig. 3(a), but whether this is due to irradiation or simply specimen variability remains uncertain. The recrystallised regions surrounding many of the primary beryllides and the small precipitates within those regions showed no difference after irradiation either. The γ'' precipitates in the grain interiors shown in Fig. 3(b) changed little in their appearance and distribution. The average size and density as quoted in Table 3, and the size distribution shown in Fig. 2(b), reveals that in fact the microstructure appears to be resistant to any significant changes in the precipitate microstructure due to irradiation to a dose level of 0.3 dpa. The diffraction patterns also reveal no substantial changes since the discrete precipitate reflections are still present at the 1/3 and $2/3[200]_{Cu}$ positions, and streaking occurs due to the presence of GP zones. Despite the lack of any noticeable changes in the microstructure due to irradiation, the irradiation at 350°C does have a strong effect on the mechanical properties of the alloy, as will be shown in later sections.

3.2.2. Tréfimétaux CuNiBe

This CuNiBe alloy was not as resistant to changes in the microstructure due to irradiation as the Hycon alloy, regardless of the pre-irradiation heat treatment. The microstructure of the solution annealed CuNiBe (HTA) specimen revealed that radiation-induced precipitation leads to a high density of small γ'' precipitates (Table 3). The diffraction patterns clearly showed that the precipitates are γ'' platelets. Their density and average size are listed in Table 3, and the size distribution is given in Fig. 4(a). Irradiation at 350°C produced a density of precipitates comparable to that measured in the prime-aged (HTE) and irradiated specimens, although with a slightly smaller mean size. Compared to that measured in the solution annealed specimens irradiated at 250°C, the higher irradiation temperature produced a higher density of precipitates. In the solution annealed (HTA) specimens irradiated at 250°C, it was reported [4] that the precipitates were difficult to measure, even when imaged in precipitate dark field using the faint streaks in the diffraction patterns. In the case of the solution annealed specimens irradiated at 350°C the precipitates were easily visible, and the size and number density could be measured more accurately. Note that compared to the Hycon alloy (Figs. 1 and 3), irradiation produced a much narrower size distribution, smaller size, and significantly higher number density. A few SFTs can be seen among the precipitates, but not well enough to confidently measure their size and number density. Narrow denuded zones along grain boundaries are present in the solution annealed specimens, and small precipitates at the boundaries are present as well. The

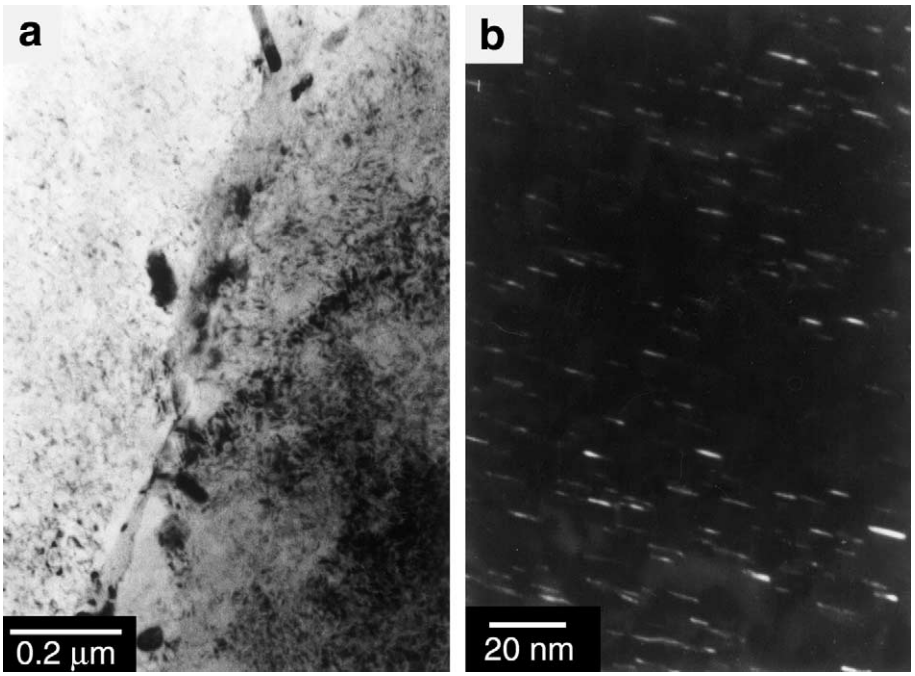

Fig. 3. Microstructure of the irradiated Hycon 3HP showing (a) precipitates at a grain boundary but no denuded zones, and (b) γ'' precipitates imaged in the precipitate dark field.

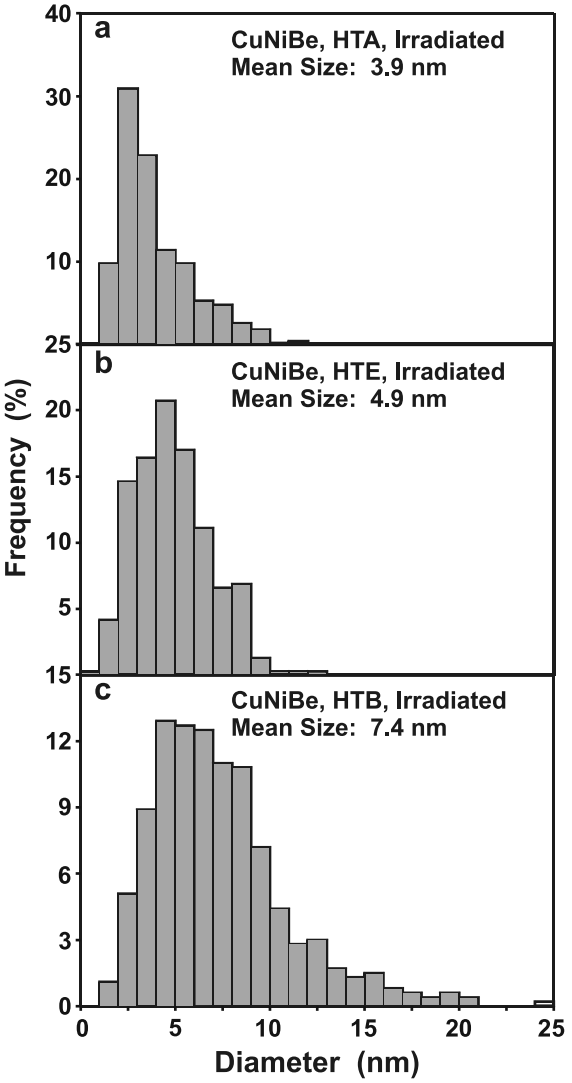

Fig. 4. Precipitate size distributions for Tréfimétaux CuNiBe alloys after irradiation showing differences between the three different heat treatments prior to irradiation. A discussion of the differences between the unirradiated and irradiated conditions is provided in the text.

primary beryllides are present also, but experience has shown that these particles are very resistant to dissolution during the high-temperature anneal, and given their size they are not expected to change significantly.

In the prime-aged (HTE) and bonding thermal cycle (HTB) conditions, the effect of irradiation is less drastic, but nonetheless visible. In Fig. 5 the denuded zones in the prime-aged (HTE) specimen have increased in size and more precipitation has occurred at the boundaries. Evidence of grain boundary migration is shown in Fig. 5(a), and some precipitation can be seen inside the denuded zones near the migrating boundary. A similar situation exists in the bonding thermal cycle (HTB) condition (Fig. 6), where the denuded zones formed during the initial heat treatment show additional evidence of having migrated during irradiation. The boundary shown in Fig. 6(a) reveals the case where very small precipitates formed at the denuded boundary, and were left behind after the boundary migrated in the direction of the three particles (see arrows). The curvature of the boundary gives an indication of the direction of boundary migration. The precipitates left behind are small, unidentified precipitates that are unlike any other precipitates present in the irradiated specimens. In addition, the original denuded zone on the boundary contains a small fraction of precipitates.

The γ'' platelets in the prime-aged and bonding thermal cycle specimens have also undergone changes during irradiation, as shown by the size and density data listed in Table 3 and the size distributions given in Figs. 4(b) and (c). In both cases irradiation at 350°C leads to an increase in precipitate diameter and more than a factor of 3 decrease in density. Compared to both the solution annealed and prime-aged conditions, the γ'' precipitates in the bonding thermal cycle specimens have the broadest size distribution both before and after irradiation. Examples of the precipitates are shown in Figs. 5(c) and 6(b), clearly illustrating the differences between the prime-aged and bonding thermal cycle conditions after irradiation.

Compared to the precipitate size and density after irradiation at 250°C [4], irradiation at 350°C resulted in larger mean size and lower density. In effect the microstructure has coarsened considerably at the higher irradiation temperature, which is also evident in that the grain boundary migration occurs more readily at $T_{irr} = 350$°C. In contrast, the Hycon alloy is relatively stable with respect to the microstructure since no discernible change is observed in the precipitate density or size distribution. Note that the average size of the γ'' platelets in the Tréfimétaux CuNiBe alloys is smaller than that measured in the Hycon alloy. Only a small fraction of the precipitates measured in the Tréfimétaux CuNiBe specimens are larger than 10 nm, and the density of precipitates in the Hycon alloy is a factor of 3 or more lower when compared individually to the three conditions of the Tréfimétaux CuNiBe after irradiation. This suggests that the larger average size of the Hycon precipitates leads to a precipitate microstructure which is more stable during irradiation.

3.2.3. *Tréfimétaux CuCrZr*

The solution annealed CuCrZr (HTA) specimen shows that radiation-induced precipitation produced a fine dispersion of very small precipitates. These precipitates possessed the 'lobe–lobe' contrast (see [4] for further details) observed in the unirradiated prime-aged (HTE) and bonding thermal cycle (HTB) speci-

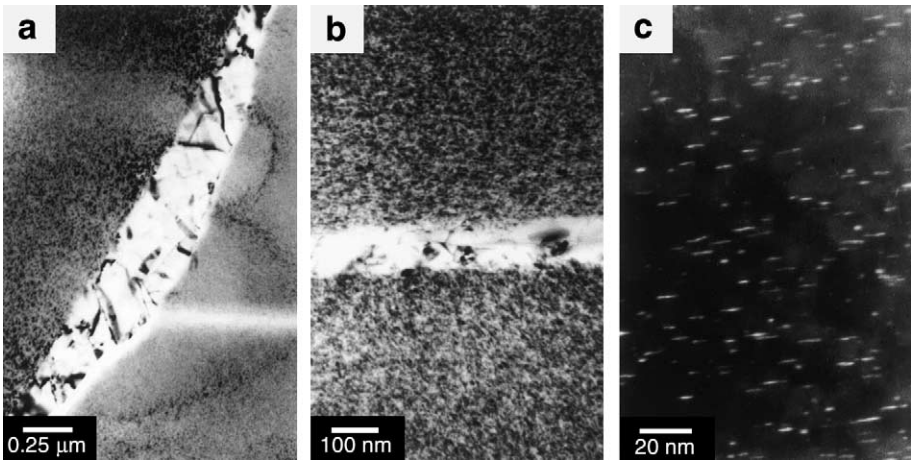

Fig. 5. Microstructure of the irradiated prime-aged CuNiBe (HTE) is shown. The micrographs in (a,b) provide two examples of the precipitate denuded zones, migration of and precipitation at the grain boundaries. A precipitate dark field image of the γ'' precipitates is shown in (c).

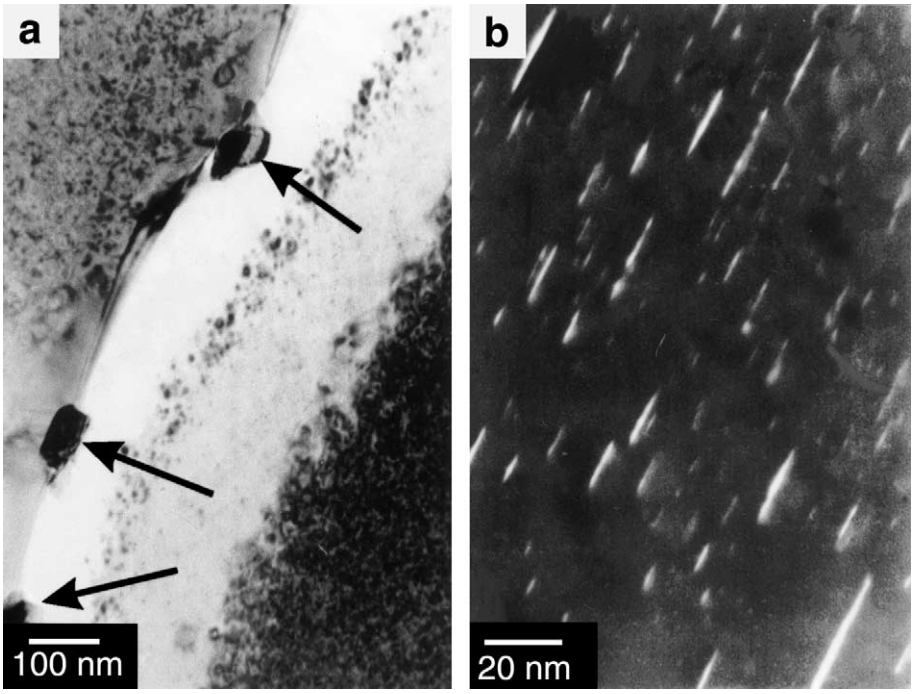

Fig. 6. Microstructure of the irradiated CuNiBe (HTB) showing (a) an example of a previously denuded boundary that has migrated and left behind small unidentified precipitates. The γ'' precipitates imaged in the precipitate dark field are shown in (b).

mens, although the mean size is smaller. None of the small round precipitates observed at $T_{irr} = 250°C$ [4] in the solution annealed specimens were observed in specimens of the same condition irradiated at 350°C. A few SFTs are scattered among the precipitates, but no estimate was made of their density. No denuded zones were found after irradiation either. Dislocation loops on the order of 100 nm diameter were observed in the solution annealed specimen. The average size of the 'lobe–lobe' precipitates and their density are given in Table 3, with the size distribution shown in Fig. 7(a). Note that irradiation at 350°C yielded a higher density of precipitates than that measured at $T_{irr} = 250°C$ [4].

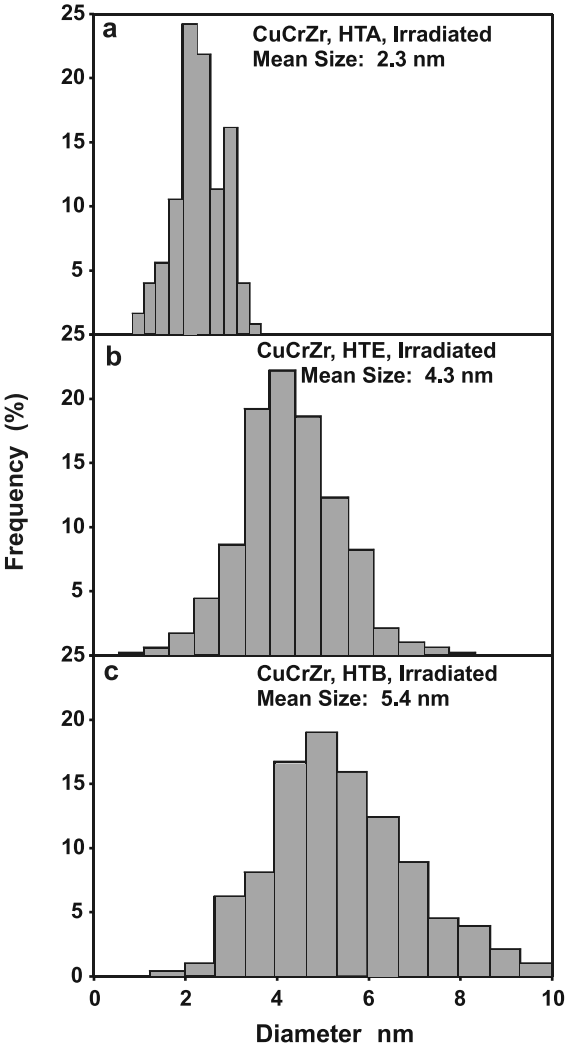

Fig. 7. Precipitate size distributions for the irradiated Tréfimétaux CuCrZr alloys for the heat treatments (a) HTA, (b) HTE and (c) HTB (see the text for clarification on the types of precipitates measured).

Irradiation of the prime-aged (HTE) and bonding thermal cycle (HTB) specimens produced significant changes in the precipitate size, density and type of precipitate. Fig. 8 gives examples of the fringed precipitates common to both types of specimens. The fringed precipitates appear to be randomly oriented and possess no visible coherency strain fields, suggesting that the precipitates in both conditions are randomly oriented, incoherent particles. Several of the precipitates in the prime-aged specimen exhibit the 'lobe–lobe' contrast more common in the unirradiated specimens, and some do not have any fringes at all, but rather are visible as round spheres or platelets. The precipitates in the bonding thermal cycle (HTB) specimens are predominantly the incoherent fringed particles, with some of the particles visible as only round spheres or platelets. Tilting to other orientations in both the prime-aged and bonding thermal cycle specimens did not reveal any edge-on platelets, so it is assumed that all of the incoherent particles are round precipitates. Based on the literature [6–9], it is likely that the precipitates are Cr-rich precipitates, however, the composition of these particles has not been investigated.

The mean size and density of the fringed precipitates are listed in Table 3, and the size distributions for both the prime-aged and bonding thermal cycle conditions are shown in Figs. 7(b) and (c). Note that the precipitate size has increased after irradiation, and is comparable to that measured for the same specimen conditions irradiated at 250°C [4]. The density of precipitates in the prime-aged condition is a factor of 3 higher than that measured in the unirradiated state and after irradiation at 250°C. In contrast to this, the density of precipitates in the bonding thermal cycle specimens is lower than or comparable to that measured in the unirradiated state and those specimens irradiated at 250°C.

In both the prime-aged and bonding thermal cycle specimens relatively large dislocation loops were formed during irradiation (an example of these loops is shown Fig. 8), just as in the solution annealed specimens. A similar observation was made in the same specimen conditions irradiated at 250°C [4]. No denuded zones were observed in either condition before or after irradiation. As mentioned previously, the cluster density was found to be $\simeq 1 \times 10^{22}$ m^{-3} for the CuCrZr alloys.

3.2.4. GlidCop™ CuAl-25

The microstructure of the DS copper alloy CuAl-25 changed very little during irradiation. The grain structure looks identical to that observed in the unirradiated specimens and in the specimens irradiated at 250°C [4]. The oxide dispersion consists primarily of spherical or polygonal morphologies with only a very few triangular particles present. The same observation was made in the case of the unirradiated specimens and the specimens irradiated at 100°C and 250°C [3,4]. The mean size and density of oxide particles are listed in Table 3, and the size distribution is given in Fig. 9. The density of defect clusters (SFT's) was found to be $\simeq 8 \times 10^{20}$ m^{-3} for the CuAl-25, much lower than that measured in the CuCrZr.

Although the density of particles is almost identical in the unirradiated state and in specimens irradiated at 350°C according to the data listed in Table 3, the mean size before and after irradiation is different. However, this particular alloy exhibits a heterogeneous microstructure with respect to the oxide particle dispersion which is a result of the internal oxidation and powder

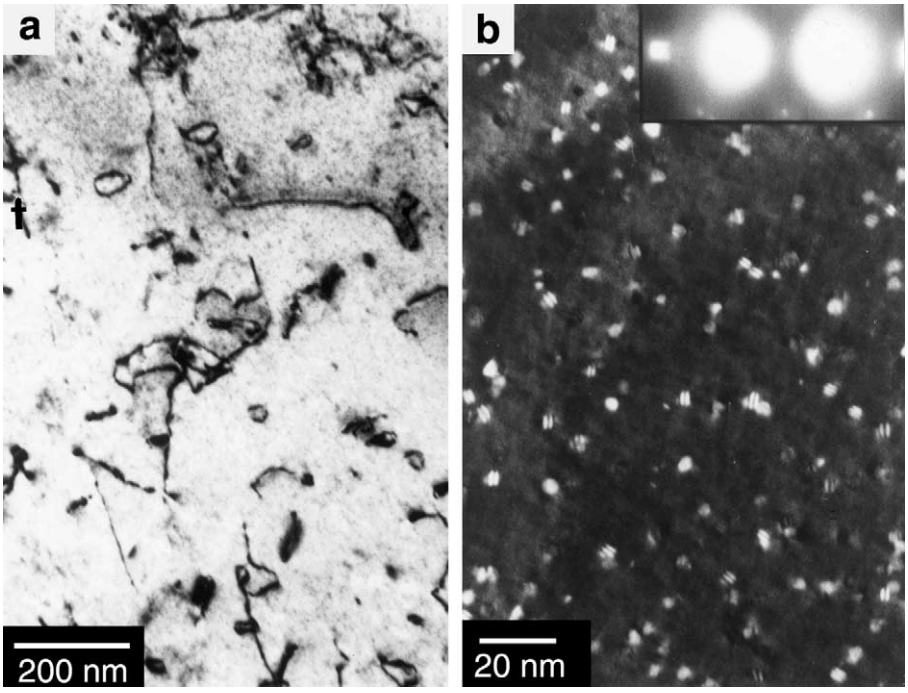

Fig. 8. Like the solution annealed CuCrZr, large dislocation loops were formed in the CuCrZr (HTE) during irradiation, examples of which are shown in (a). The WBDF image shown in (b) is of the fringed precipitates that dominate the microstructure.

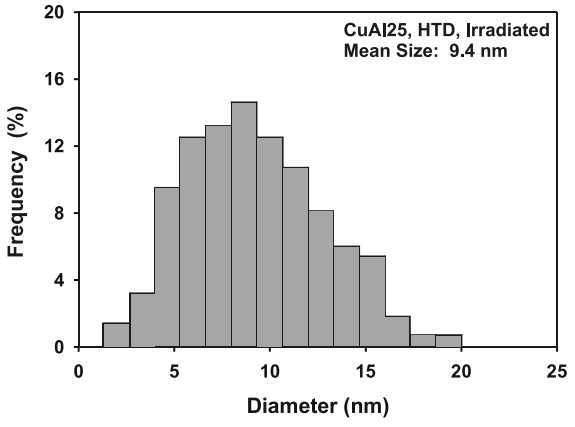

Fig. 9. Precipitate size distribution for the irradiated CuAl-25 shows that the oxide particles range in size from 2 to 20 nm in diameter.

metallurgy approach to making the alloy. As has been shown in previous work by the authors [4,10], the average size can range from 5 to 10 nm depending on the area examined, and the density can vary by a factor of 100, that is from 10^{20} to 10^{22} m^{-3}. Overall this material has proven to be the most resistant microstructurally to radiation-induced changes of any of the alloys examined, a fact that is reflected in the mechanical properties.

4. Pre- and post-irradiation electrical resistivity

Irradiation of CuNiBe alloys at 350°C caused a significant decrease in the electrical resistivity of the specimens irrespective of the heat treatment (Table 4). The electrical resistivity of the prime-aged (HTE) and bonding thermal cycle (HTB) conditions for CuCrZr also exhibited a substantial decrease after irradiation. In each case it appears that the overall coarsening observed in the microstructure (Table 3) leads to an improvement in the electrical conductivity. The CuCrZr alloy shows the largest improvement in electrical conductivity, suggesting that a larger proportion of the Cr and/or Zr remained in solution compared to the Tréfimétaux CuNiBe alloys. The one exception is that the electrical resistivity of the Hycon alloy was essentially unchanged by irradiation, which agrees qualitatively with the microstructural analysis revealing little change in the Hycon alloy due to irradiation.

5. Pre- and post-irradiation mechanical properties

The influence of 350°C irradiation temperature and test temperature is particularly noticeable in the CuNiBe alloys, all of which exhibited very poor elongations both before and after irradiation. The CuCrZr, though much lower in overall strength, maintained an acceptable level

Table 4
Electrical resistivity and conductivity for copper alloys irradiated at 350°C to a dose level of 0.3 dpa

Materials	Heat treatment	Irradiation dose (dpa)	Relative resistivity	Relative conductivity
OFHC	550°C, 2 h	Unirr	1	1
CuNiBe	A	Unirr	3.129	0.320
CuNiBe	E	Unirr	2.345	0.426
CuNiBe	B	Unirr	2.374	0.421
Hycon 3HP	'Prime-aged'	Unirr	1.547	0.646
Cu–Cr–Zr	E	Unirr	1.625	0.615
Cu–Cr–Zr	B	Unirr	1.403	0.713
CuNiBe	A	0.3	2.062	0.485
CuNiBe	E	0.3	1.997	0.501
CuNiBe	B	0.3	1.893	0.528
Hycon 3HP	'Prime-aged'	0.3	1.523	0.657
Cu–Cr–Zr	E	0.3	1.294	0.773
Cu–Cr–Zr	B	0.3	1.183	0.845

of uniform and total elongation both before and after irradiation. The irradiated CuAl-25 exhibited a plastic uniform elongation of 2–3%. The results of mechanical properties are briefly presented in the following sections. Tables 5 and 6 provide a summary of the tensile results for the unirradiated and irradiated specimens, respectively.

For comparison purposes, specimens of annealed [550°C/2 h] OFHC–Cu were also irradiated at 350°C to a dose level of 0.3 dpa and were tensile tested at 350°C. The tensile results are included in Tables 5 and 6 and the corresponding stress–strain curves are shown in Fig. 10. It should be noted here that the neutron irradiation even at this relatively high temperature (0.46 T_m where T_m is the melting temperature) and to a relatively low dose level of only 0.3 dpa causes a significant decrease in the ductility of the OFHC–Cu.

5.1. CuNiBe

The unirradiated solution annealed (HTA) Tréfimétaux CuNiBe has a very low yield strength and high elongation, with a work hardening ability comparable to that of pure copper. The bonding thermal cycle (HTB) and bakeout simulation (HTC and HTC′) treatments produce an alloy that still possesses reasonable ductility and work hardening even when tested at 350°C. However, the Hycon 3HP surprisingly exhibits very low ductility and work hardening when tested at 350°C. Fig. 11(a) provides a comparison between the Hycon and the

Table 5
Tensile results for unirradiated OFHC–Cu and copper alloys with the pre-irradiation heat treatments described in Table 2

Material	Heat treatment	$\sigma_{0.05}$ (MPa)	$\sigma_{0.2}$ (MPa)	σ_{max} (MPa)	ε_u^p (%)[a]	ε_{total} (%)
OFHC–Cu	550°C/2 h	18	23	95	37.8	48.0
CuNiBe	A[b]	90	100	363	45.9	55.3
CuNiBe	A	118	125	375	50.9	53.0
CuNiBe	B	430	468	615	8.2	10.5
CuNiBe	C	475	525	635	5.1	5.8
CuNiBe	C′	518	560	638	10.0	11.1
CuNiBe	Hycon[c]	495	550	583	1.3	2.6
CuCrZr	A	69	76	165	21.3	26.5
CuCrZr	B	123	138	214	17.2	19.0
CuCrZr	C	169	178	243	15.2	18.3
CuCrZr	C′	184	183	244	12.5	14.5
CuCrZr	E	178	185	245	14.7	17.5
CuAl-25	D[b]	235	250	255	1.5	28.0
CuAl-25	D′[b]	233	241	245	1.8	15.3

[a] ε_u^p refers to the uniform plastic strain. Tests were conducted at 350°C.
[b] Round specimens, 3 mm diameter gauge.
[c] Longitudinal direction, heat number 33667.

Table 6
Tensile results for OFHC–Cu and copper alloys irradiated at 350°C to 0.3 dpa with the pre-irradiation heat treatments described in Table 2

Material	Heat treatment	$\sigma_{0.05}$ (MPa)	$\sigma_{0.2}$ (MPa)	σ_{max} (MPa)	ε_u^p (%)[a]	ε_{total} (%)
OFHC–Cu	550°C/2h	27	37	86	12.0	17.0
CuNiBe	A[b]	510	556	580	0.7	4.2
CuNiBe	B	225[c]	–	–	–	–
CuNiBe	E[d]	–	–	–	–	
CuNiBe	Hycon[e]	405[c]	–	–	–	–
CuCrZr	A	183	190	267	15.4	44.0
CuCrZr	B	161	174	234	12.4	14.5
CuCrZr	E	172	186	242	12.2	14.5
CuAl-25	D[b]	225	245	255	3.4	17.5
CuAl-25	D′[b]	196	203	208	2.0	12.3

[a] ε_u^p refers to the uniform plastic strain. Tests were conducted at 350°C.
[b] Round specimen, 3 mm diameter gauge.
[c] Broke prematurely.
[d] Specimen broke during mounting in test machine.
[e] Brush Wellman, heat 33667.

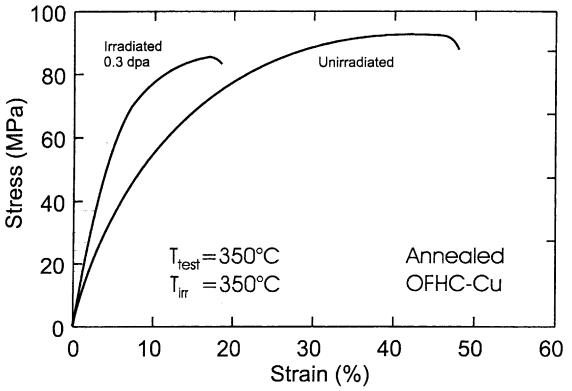

Fig. 10. Stress–strain curves for the unirradiated and irradiated OFHC-copper tested at 350°C. Note that irradiation with neutrons, even at relatively high temperature caused a significant decrease in ductility.

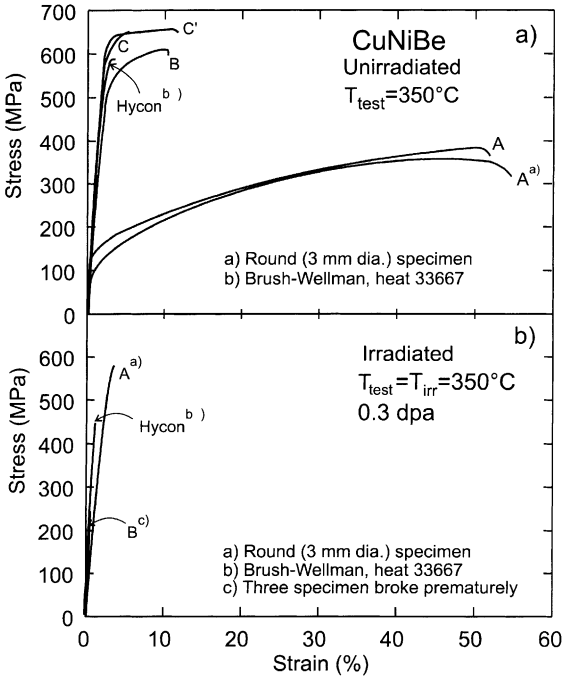

Fig. 11. Stress–strain curves for CuNiBe alloys with heat treatments A, B, C and C′ (see Table 2) tensile tested at 350°C in (a) unirradiated and (b) irradiated conditions. Note that the ductility of the Hycon alloy is significantly lower than that of the Tréfimétaux (HTB) even in the unirradiated condition. Clearly, irradiation causes signficant levels of embrittlement in all of the alloys.

Tréfimétaux CuNiBe given the bonding thermal cycle treatment (B) and the solution annealing treatment (A). Clearly the Hycon 3HP alloy does not exhibit the same behaviour as the Tréfimétaux CuNiBe specimens, despite a similar level of strength. In addition, Fig. 11(a) also shows the effect that the bakeout treatment (C, C′) has on the properties of the Tréfimétaux CuNiBe. Although well below the 475°C aging temperature used for this alloy, holding the specimens at 350°C for 100 h obviously produces a change in the microstructure that leads to a noticeable increase in yield strength and a slight increase in the ultimate strength.

Irradiation at 350°C of the various CuNiBe specimens leads to severe embrittlement of both the Tréfimétaux CuNiBe alloy and the Hycon 3HP. The data in Table 6 show that the only condition exhibiting measurable ductility was the irradiated solution annealed specimen. The irradiation-induced precipitation leads to a microstructure with a high precipitate

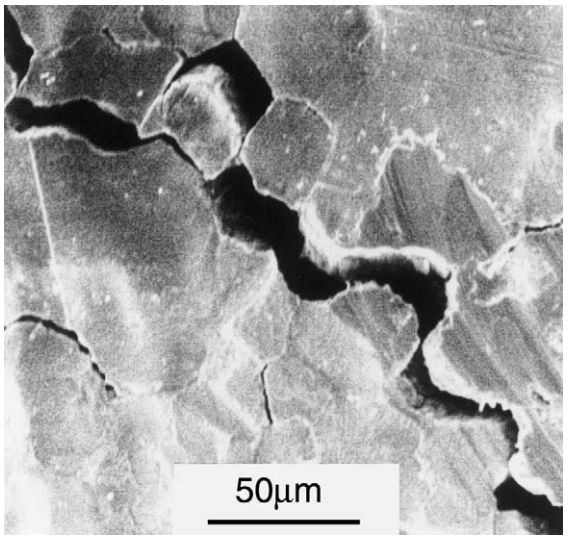

Fig. 12. Micrograph of the gauge surface of the irradiated (after heat treatment B) specimens near the fracture surface demonstrating the brittleness of these alloys. Note that a grain in the gauge section near the fracture surface has been pulled apart from its neighbouring grains.

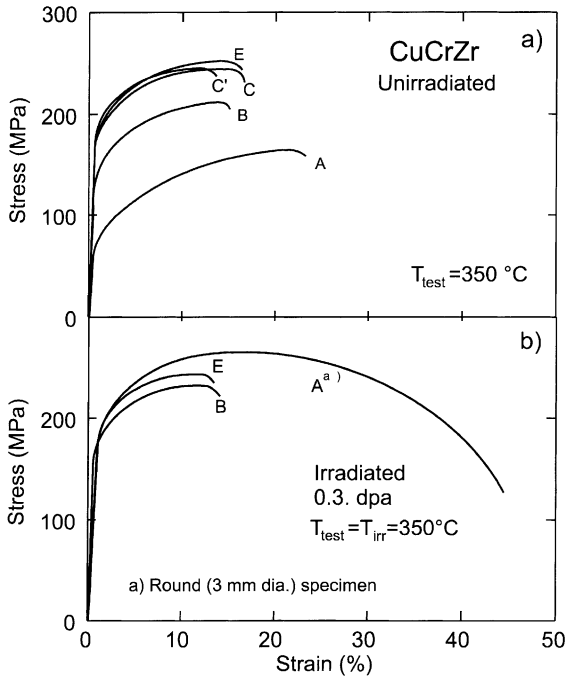

Fig. 13. Stress–strain curves for Tréfimétaux CuCrZr alloy with heat treatments A, B, C, C′ and E (see Table 2) tensile tested at 350°C in (a) unirradiated and (b) irradiated conditons.

density, but yet allowed a uniform elongation of 1.3%. The tensile curve shown in Fig. 11(b) for the solution annealed specimen illustrates the point that although possessing sufficient strength, this condition still allows very little work hardening to occur. As indicated in Fig. 11(b), three of the specimens given the bonding thermal cycle treatment (HTB) broke prematurely at an average stress of 225 MPa, almost half of the unirradiated yield strength. The prime-aged specimens broke during mounting in the test frame, further illustrating the extreme embrittlement of these materials. The Hycon alloy, although breaking at a much higher load, also failed prematurely before reaching the point where the 0.2% offset yield stress could be measured. The fracture surface of the irradiated HTB CuNiBe specimen demonstrated that the failure occurred along the grain boundaries. The gauge surface of the specimen is shown in Fig. 12, revealing that a crack is cleanly following the path along the grain boundaries.

5.2. CuCrZr

The CuCrZr exhibits reasonable work hardening and uniform elongation regardless of the initial state of the material, as shown in Fig. 13(a). Despite the great difference in microstructures between the specimens given the solution annealing, prime-aging or bonding thermal cycle, the CuCrZr alloys do not exhibit the same degree of strengthening from the precipitates as do the CuNiBe alloys. This is due to the fact that there is an order of magnitude higher precipitate density in the CuNiBe alloys, as well as large coherency strains that further enhance the strengthening effect of the γ'' precipitates and GP zones. The bakeout simulation produces some change in the strength of the specimens initially given the bonding thermal cycle treatment, but had no effect on the prime-aged CuCrZr (Fig. 13(a)).

Irradiation and testing at 350°C produced only minor changes in the strength and ductility of the CuCrZr. As can be seen in Fig. 13(b), the irradiation-induced precipitation in the solution annealed material produces comparable strength to that measured in the prime-aged and bonding thermal cycled specimens. The higher ductility may be due to the fact that the tested specimens were a round geometry as opposed to the sheet specimens used for the other specimens. A fracture surface from the CuCrZr (HTE) specimen is shown in Fig. 14, revealing that the failure mode is a ductile, knife-edge failure.

5.3. GlidCop™ CuAl-25

The CuAl-25 proved to be resistant to any significant changes in the overall strength and ductility during irradiation. Tensile curves are provided in Fig. 15

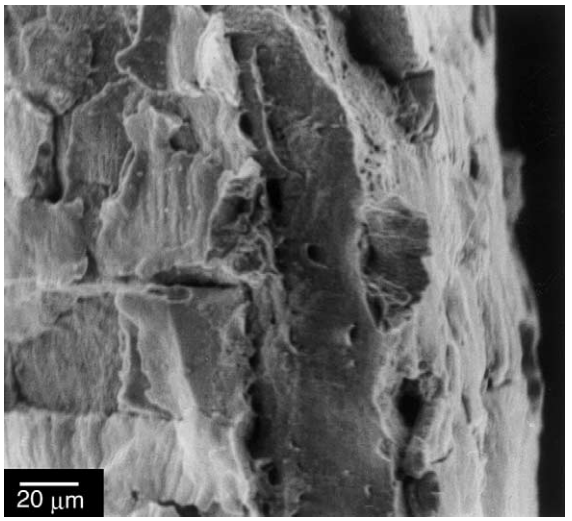

Fig. 14. Fractograph of the Tréfimétaux CuCrZr specimen with heat treatment E (Table 2) and tested in the irradiated condition showing that the specimen failed in a ductile manner yielding a 'knife-edge' fracture appearance.

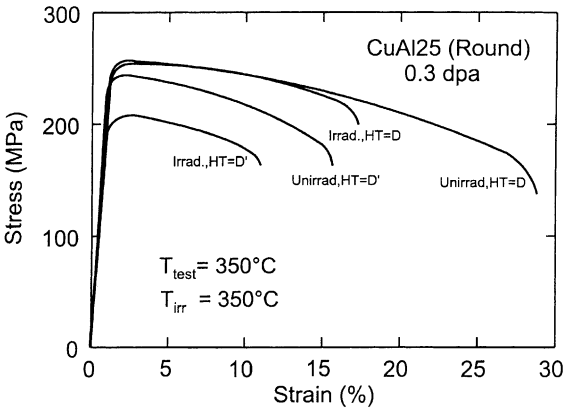

Fig. 15. Stress–strain curves for the unirradiated and irradiated CuAl-25 alloy tested at 350°C. Note that all specimens exihibit very little uniform elongation, a consequence of the poor work hardening ability. All specimens tested were of the round geometry (3 mm dia). D and D′ refer to different heat treatments (see Table 2).

illustrating the effect of the annealing treatment (HTD) on the properties of the unirradiated CuAl-25. Although the curves seem to suggest that the material is stronger after annealing, the data tabulated in Table 5 show in fact the only difference is that the annealed specimen has a higher total elongation. Note that except for the Hycon alloy, the uniform elongation and work hardening ability for the dispersion strengthened alloy is very low compared to that of the other unirradiated alloys.

Irradiation at 350°C leads to irradiation-induced softening in the as-wrought (HTD′) CuAl25, whereas the strength of the annealed CuAl-25 (HTD) is relatively stable (Fig. 15, Table 6). Both the HTD and HTD′ conditions show a slight improvement in the uniform elongation, but the overall work hardening ability has not improved significantly.

6. Discussion

Irradiation at 350°C does lead to noticeable changes in the microstructure of all of the alloys except the GlidCop^{TM}. Irradiation also produced quite significant changes in the electrical resistivity of both the Tréfimétaux CuNiBe and CuCrZr alloys. The Hycon alloy, however, was resistant to any measurable changes in the microstructure, which was reflected also in the electrical resistivity results. Large dislocation loops were produced in the CuCrZr alloys due to the presence of the alloying elements. Their effect was also evident in the defect cluster density, which was much higher than that measured in the CuAl-25 and previously in the OFHC–Cu [10]. This effect of alloying elements points to fundamental interaction between the alloying elements and radiation produced defects. The presence of such loops or defect clusters could not be confirmed in CuNiBe due to the high precipitate density. Although stable microstructurally, the tensile results suggest that the CuAl-25 should not be irradiated in cold-worked conditions since a significant loss of strength may occur due to irradiation enhanced recovery.

This study has illustrated clearly that the irradiated CuNiBe alloys are very susceptible to some form of embrittlement that occurs when tested at temperatures above 250°C, as previously reported by Singh et al. [4] and by Zinkle and Eatherly [11]. Irradiation serves to exacerbate the problem at elevated test temperatures compared to the unirradiated state, but the reason remains unclear at present. The observation (Fig. 5(a)) that the grain boundaries migrated and left behind small unidentified precipitates may provide part of the answer, i.e., the formation of precipitates at the boundary and in the denuded zones by radiation-induced dissolution and re-precipitation of the Be and Ni. This redistribution of the Be and/or Ni to the grain boundaries may be a source of the embrittlement exhibited in the irradiated CuNiBe alloys, however, at present segregation of other impurities cannot be ruled out. In addition to the segregation to grain boundaries, Singh and co-workers [4] have suggested that the occurrence of irradiation-induced changes in the grain interiors may make them significantly stronger than the

grain boundaries and the adjacent denuded zone. Consequently, this may lead to a situation where the initiation and localisation of the plastic flow in the grain boundary region may cause separation of grains without any significant amount of deformation in the grain interiors.

Singh and co-workers [4] reported that irradiation at 250°C of the same alloys and conditions leads to only minor changes in the electrical resistivity. They also reported that giving CuNiBe a bakeout simulation (350°C for 100 h) produced an improvement in the electrical conductivity. Comparing those results to the current data after irradiation at 350°C demonstrates that the bakeout simulation produces comparable changes in the resistivity, so the effect of irradiation is somewhat overshadowed by the influence of temperature.

Taking into account the results presented previously for the alloys irradiated at 250°C [4,11], it is clear that in terms of response to irradiation above 250°C, GlidCop™ and CuCrZr perform better than the CuNiBe alloys. However, both of these alloys are lacking when strength is considered. The electrical resistivities of the GlidCop™ and CuCrZr are generally superior to those of the CuNiBe alloys, although there is some overlap between the two precipitation strengthened alloys depending on the initial starting state. Based strictly on electrical resistivity/conductivity and ductility considerations, the CuNiBe alloy has proven to be an unlikely candidate for fusion applications where the irradiation temperature exceeds $\simeq$250°C. To put this in perspective, one must also consider that the neutron spectrum of the ITER reactor will encompass a predominantly 14 MeV neutron spectrum, with higher recoil energies and transmutation rates. This more severe environment may impose additional uncertainties on the use of CuNiBe alloys.

7. Conclusions

On the basis of the changes measured in the microstructure, mechanical properties, and electrical resistivity of the PH and DS copper alloys, the following conclusions can be drawn.

- The DS copper alloy CuAl-25 exhibits the greatest resistance to radiation-induced changes in microstructure and mechanical properties at $T_{irr} \geqslant 250$°C.
- The different heat treatments given to the CuNiBe and CuCrZr alloys make little difference in their mechanical properties after irradiation at 350°C to 0.3 dpa.
- Irradiation at 350°C leads to greater changes in the precipitate microstructure in the grain interiors and at or near the grain boundaries than observed at 250°C.
- Irradiation of solution annealed CuNiBe and CuCrZr leads to radiation-induced precipitation that can produce strength levels near to that of the unirradiated specimens with heat treatments HTB and HTE.
- Radiation-induced dissolution and re-precipitation change the precipitate characteristics in both CuNiBe and CuCrZr alloys. In addition, the radiation-induced precipitate dissolution may be responsible for promoting segregation of alloying and impurity elements in the CuNiBe, particularly at and near the grain boundaries.
- CuCrZr appears to offer advantages over the CuNiBe because there remains a reasonable level of ductility and work hardening even after irradiation, however, the low strength is a limitation that has to be considered.
- The severe loss of ductility in the CuNiBe alloys due to neutron irradiation, regardless of the initial starting state or composition, may present serious problems regarding their application in an intense flux of 14 MeV neutrons. The actual mechanism(s) responsible for the observed decrease in ductility in the post-irradiated CuNiBe alloys has not been firmly identified. It seems very likely, however, that the ballistic resolution and irradiation enhanced diffusion and segregation may play an important role.

Acknowledgements

The present work was partly funded by the European Fusion Technology Programme. The authors wish to thank Steven J. Zinkle (Oak Ridge National Laboratory) for providing the CuNiBe alloy Hycon 3HP™ and B.F. Olsen, N.J. Pedersen and J.L. Lindbo for technical assistance. D.J.E. would like to thank Risø National Laboratory for the support and assistance during his visit. His work was also partly supported by the US Department of Energy under contract DE-AC06-76RLO 1830 with the Battelle Memorial Institute at the Pacific Northwest National Laboratory.

References

[1] ITER Joint Central Team, J. Nucl. Mater. 212–215 (1994) 3.
[2] J.W. Davis, D.E. Driemeyer, J.R. Haines, R.T. McGrath, J. Nucl. Mater. 212–215 (1994) 1353.
[3] D.J. Edwards, B.N. Singh, P. Toft, M. Eldrup, J. Nucl. Mater. 258–263 (1998) 978.
[4] B.N. Singh, D.J. Edwards, M. Eldrup, P. Toft, J. Nucl. Mater. 249 (1997) 1.

[5] A. Guha, in: E. Ling, P.W. Taubenblat (Eds.), High Conductivity Copper and Aluminum Alloys Conference Proceedings, The Metallurgical Society of AIME, Los Angles, CA, 1984, p. 133.
[6] M.F. Ashby, L.M. Brown, Philos. Mag. 8 (1963) 1083.
[7] N.Y. Tang, D.M.R. Taplin, G.L. Dunlop, Mater. Sci. Technol. 1 (1985) 270.
[8] Z. Rdzawski, J. Strobrawa, Scripta Metall. 20 (1986) 341.
[9] R.W. Knights, P. Wilkes, Metall. Trans. 4 (1973) 2389.
[10] B.N. Singh, A. Horsewell, P. Toft, D.J. Edwards, J. Nucl. Mater. 224 (1995) 131.
[11] S.J. Zinkle, W.S. Eatherly, Fusion Materials Semiannual Progress Report, DOE/ER-0313/20, 1996, p. 207.